https://doi.org/10.1016/j.apsusc.2020.146031

Plasma charging effect on the nanoparticles releasing from the cavitation bubble to the solution during nanosecond Pulsed Laser Ablation in Liquid

Marcella Dell'Aglio[1], Alessandro De Giacomo[1,2]

1. CNR-NANOTEC, c/o Chemistry Department, University of Bari, Via Orabona 4, 70126 Bari, Italy
2. Chemistry Department, University of Bari, Via Orabona 4, 70126 Bari, Italy

Abstract.

The laser induced plasma during the nanosecond Pulsed Laser Ablation in Liquid (PLAL) plays a crucial role in the nanoparticles (NPs) formation and charging. It was demonstrated that during the plasma phase evolution, once the NPs are formed, they are charged with the excess of plasma electrons. Immediately after the plasma phase extinguishes, the NPs will be released in the induced vapor bubble, generated by the fast energy exchanges between the plasma and the liquid. The excess of charge in the NPs preserves them from the agglomeration during the bubble evolution and can induces an electrostatic pressure able to eject the particles outside the cavitation bubble.

In this work, the plasma charging effect on the particle releasing in solution, during the bubble evolution, has been investigated. Temporal evolution of laser induced bubble on silver target immersed in water has been measured with the shadowgraph technique. Then, starting from the experimental bubble radius evolution, the releasing of the NPs from the cavitation bubble to the liquid has been modeled by comparing the electrostatic pressure of the charged NPs cloud and the pressure of the cavitation bubble. The following discussion proposes a new insight of the mechanism of NPs releasing in solution.

Keywords: Pulsed Laser Ablation in Liquid (PLAL), Laser Ablation Synthesis in Solution (LASIS), NPs releasing, NP formation, Cavitation bubble.

1. Introduction.

Pulsed Laser Ablation in Liquid (PLAL) or Laser Ablation Synthesis in Solution (LASIS) is getting a growing interest for the production of colloidal solution of noble metal nanoparticles (NPs) as it allows the production of extremely pure NPs without the necessity of chemical stabilizers. The possibility of producing ultra-pure NPs has pushed a great interest in the field of analytical chemistry because the use of such NPs enables the possibility of exploiting plasmon enhanced laser ablation for elemental analysis [1]. The basic mechanisms involved in the formation of NPs have been largely discussed in literature and although different hypothesis has been reported, what has been clearly demonstrated is that the PLAL techniques involves the following processes [2, 3]: Laser matter interaction, plasma induction, the formation of the cavitation bubble and the releasing of nanostructure in solution. In previous works we have demonstrated, both theoretically [4] and experimentally [5], that the plasma phase plays a crucial role in the formation and in the stabilization of the NPs during ns-PLAL as a consequence of the high density of the plasma and of the charging effects. Starting from these results, in this paper we focus our efforts in characterizing the releasing of the NPs from the cavitation bubble to the solution during ns-PLAL.

In Ref [5] the spatial characteristics of the plasma have been discussed in order to show the temperature and density distribution during the plasma evolution. In that paper has been shown that

the plasma is characterized by suitable thermodynamic conditions for the NPs formation and that, whatever is the kinetics of growth of the NPs in the plasma phase, the free electrons can charge the surface of the NPs in picosecond time scale. The latter observation, already estimated with a theoretical model in Ref.s [4, 6], suggests that the produced NPs hold an excess of electrons that indeed can play an important role in preserving the NPs aggregation during the cavitation bubble evolution. In this paper, the importance of the charging effect on the NPs is investigated in order to study one of the most obscure stages of the PLAL process that is the releasing of the NPs in solution. The transfer of the NPs from the cavitation bubble to the solution is very difficult to be determined experimentally. Some works have reported the presence of NPs in the solution already during the bubble expansion [7]. Others observations suggest that the most of the NPs are released in the solution during the collapse stage [8]. Other papers report the presence of NPs inside the cavitation bubble during the entire bubble evolution [8-9]. In spite of so many and various observations, at the best of our knowledge, there is still not a theory who is devoted to explain how the NPs are released in the solution and why they do not attach themselves for forming aggregate in order to decrease their surface energy. As a matter of fact, when the excess of electrons on the NPs is taken into consideration, a repulsion force between the NPs should be expected that, from one hand preserves the aggregation and, on the other hand, induces an electrostatic pressure at the surface of the cavitation bubble which directly depends on the number of NPs and on the number of charges. Based on this observations we propose the investigation of the electrostatic pressure of the charged NPs and the effect of this pressure on the ejection of the NPs from the cavitation bubble.

As a consequence of the complexity of the real system, some rough simplifications has been assumed in order to investigate, at least qualitatively, the potential effect of the electrostatic repulsion of charged NPs on NPs releasing in solution during ns-PLAL and they are: the vapor in the bubble is considered neutral (we neglect the effect of water molecule dissociation as well as the presence of ions in the babble), the distribution of the NPs is taken into account with a single average size, the pressure of the bubble has been considered homogeneous. Although the present approach needs to be improved for a quantitative description of the phenomenon, it shows the effect of the charging on NPs releasing from the bubble to the solution in a simple and intuitive way.

2. Scientific background on noble metal NPs formation in plasma and charging of NPs

The formation of NPs in the plasma phase has been previously reported by many authors [10, 11, 12] and has been mainly related to the condensation/evaporation balance and in turn to the plasma temperature. On the basis of the temperature and density maps reported in a previous paper [5] it has been possible to investigate the phenomena leading to the NPs formation in the different zones of the plasma during ns-PLAL.

For instance, in the border of the plasma, due to the transfer of energy from the plasma to the surrounding liquid a cooling of this portion of plasma should be expected. Being the border of the plasma characterized by instabilities, the process of condensation would lead to particles with a casual size distribution. As a matter of fact, because of the fast cooling, the backward process of evaporation is negligible in comparison with the condensation and the particle size is determined mainly by the atomic number density at the plasma border [13].

Another possibility is that NPs grow in the plasma bulk. In this frame the zone of the plasma with lower temperature and high density holds suitable conditions for particle growth. By the observation of temperature spatial distribution reported in Ref. [5] it is visible that in the bulk of the plasma, where the density is higher, the temperature decreases more than 30% with respect to the averaged temperature of the plasma. Moreover, since the pressure is in the order of several tens to hundreds of bars, the condensation can occur at higher temperature than that of the standard boiling point of metals. At this condition, being the temperature high enough to induce also surface evaporation, the growth of the NPs is balanced by the evaporation and the equilibrium of these

processes, condensation and evaporation, establishes the final particle size [13]. The experimental conditions of the plasma suggest also to consider the growth mechanism based on the electrostatic growth [4-6]. This mechanism, commonly studied for dusty plasmas [14], supposes the following steps:

1) Due to the high initial high density, small clusters of atoms are formed by condensation during the ablation process [4,6].

2) Because the electrons are faster than all the other particles in the plasma they negatively charge the seed clusters.

3) Ions implant on the cluster surface because of the electrostatic attraction inducing the growth of the NPs.

Initially the electrostatic growth is faster than the evaporation as reported in Ref. [4], but as mentioned above in the case of thermodynamic condensation, being the evaporation rate dependent on the NP surface area, when the NP reaches a certain size, the growth is balanced by the evaporation and the NPs size is established. In all the cases, when the NPs exit from the plasma domain their growth dynamic is quenched.

During PLAL for the production of noble metal NPs, condensation/evaporation and the electrostatic growth in the bulk of the plasma would justify the experimental observations, where the most of the particles have a narrow size distribution around 10 nm and spherical shapes. On the contrary, processes occurring at the border of the plasma with the background liquid, that are characterized by instabilities, leads to bigger NPs of various size and eventually not only of spherical shape. As a matter of fact, many experimental observations [15, 16] report the formation of two kind of NPs, the spherical one usually with a size in the order of 10 nm, and a small fraction of bigger NPs also with different shape. For practical use, the latter particles types are generally removed by centrifugation of the obtained colloidal solution.

Finally, whatever is the kinetics of growth of the NPs in the plasma phase, the free electrons can charge the NPs in picosecond time. This suggests that the produced NPs hold an excess of electrons [17, 18], thus preserving individual spherical NPs from massive aggregation, in agreement with the experimental observations. The main mechanisms involved in the disappearing of free electrons in the plasma phase are the following:

a) three body recombination

$$A_l + e^-_{(E_{e^-})} \underset{K^{3b}}{\overset{K^{ion}}{\Leftrightarrow}} A^+ + e^-_{(E_{e^-} - E'_{e^-} - E_{ion} + E_l)} + e^-_{(E'_{e^-})}$$

with characteristic time:

$$\tau_{3b} = 2.56 \cdot 10^{21} \frac{T^{4.5}}{N_e^2} \qquad \text{eq.1}$$

b) charging

$$A_m^{-n} + e^- \Leftrightarrow A_m^{-(n+1)}$$

with characteristic time:

$$\tau_{ch} = 34.45 \frac{T^{0.5}}{rN_e} \qquad \text{eq.2}$$

where r is the particle radius in m, while N_e is the electron number density in m^{-3} and T the plasma temperature in K.

The charging effect was studied in details in Ref[5] and it can be summarized with Fig.1 where free-electrons charging time and the three body recombination time, are shown as function of plasma electron number density at different temperatures. By the inspection of the Fig.1 we can outline that, while the charging process depends moderately on the plasma temperature, in the case of the three body recombination process this dependence is more evident. By the plot of Fig.1 it is possible to see that for the typical plasma electron density of a ns-PLAL [16, 19], between 10^{22} m^{-3} and 10^{24} m^{-3}, at the reported temperatures, the charging effect is faster than the three body recombination. This means that, although the recombination is not so much affected by the charging process because the latter involves few electrons with respect to the recombination, the charging of particle in the plasma at the experimental condition used in PLAL, occur immediately and the consequent effect on the characteristics of the NPs cannot be neglected.

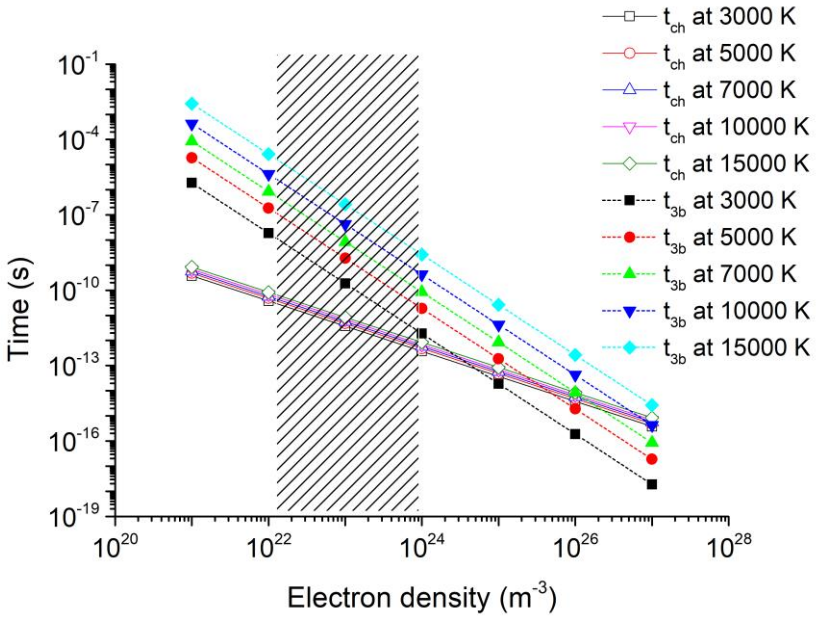

Fig. 1 Characteristic times of three body recombination (t_{3b}) and charging (t_{ch}) elementary processes as function of electron number density at different plasma temperatures. Hatched area corresponds to typical value of electron number density at plasma condition during PLAL process.

3. Materials and methods

The production of AgNPs and the shadowgraph measurements were performed by employing a ns pulsed laser (Quantasystem, PILS-GIANT, 6 ns pulse duration) operating with the second harmonic (532 nm), a repetition rate varying between 1 and 10 Hz and with an energy varying between 217 mJ and 50 mJ, in dependence of the performed experiment.

A stainless steel chamber has been employed for the production of AgNPs. The chamber was filled with 400 ml of deionized water, the target was placed on the rotating holder with the possibility of 10 mm axial movement (backward and forward) and the laser was focused onto the target surface by a 4.0 cm focusing lens inserted inside the spacer tube on the opposite position with respect to the target (Fig. 2). A sapphire optical windows placed on the wall of the chamber allow detecting signal.

For performing the shadowgraph measurements of the laser induced bubble during the AgNPs production, a collimated light source obtained by a set of lenses and a fast ICCD detection system (New iStar, Andor) coupled with a pulse generator (Stanford inc. DG 535) for the laser pulse-ICCD synchronization have been employed. The shadowgraph images were acquired at 90º with respect to the laser pulse direction keeping the target fixed in order to avoid formation of some

gas bubbles along the optical path between the target and the lens collecting the shadow. The laser focal position onto the target surface as well as the water were changed after each measurement in order to perform measurements on flat target and fresh water, respectively. The focal plane of the laser beam was put inside the target, in order to get a laser crater on the target with a diameter of 1 ± 0.2 mm. In Fig. S1, the craters induced with different laser energies employed for the experiments of this work are shown. All shadowgraph images were acquired by using the kinetic mode of the ICCD, with a gate width of 20 μs and 5 accumulations for each image. The shadowgraph images of the cavitation bubble are acquired by using a laser frequency of 2 Hz, so that the nanoparticles have more time to diffuse between two successive laser shots reducing the number of AgNPs stationing in the beam waist.

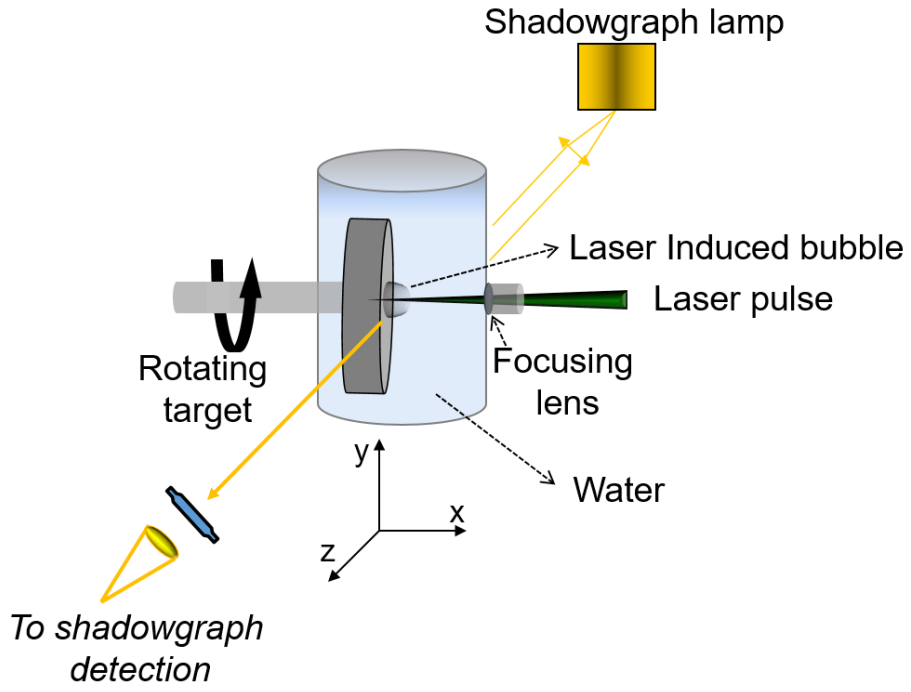

Fig. 2 Experimental set-up

The silver target employed in the experiment was purchased from Kurt J. Lesker Company (99.99% pure pellet).

AgNPs colloidal solution, as well as the shadowgraph measurements, were produced by adding to the MilliQ water also 100 μM of KCl, in order to obtain a more stable AgNPs solution adding the minimum quantity of salt.

The Surface Plasmon Resonance (SPR) absorption spectroscopy of the AgNPs colloidal solutions was performed with an Ocean Optics (USB2000+XR) spectrometer equipped with a continuous light source (Mini Deuterium Halogen Light Source DT-Mini-2-GS).

In order to obtain the concentration and the size of the AgNPs, SPR spectra have been used by building appropriate calibration curves. The calibration curves are: a) absorbance at the maximum wavelength ($A_{\lambda max}$) as function of concentration (at fixed size) in order to obtain the extinction coefficient at the maximum of absorbance at each employed NPs size and b) wavelength at the maximum of absorbance (λ_{max}) as function of NPs size at fixed concentration, in order to obtain a relation between the λ_{max} redshift and the NPs size, as already reported in ref. [20, 21, 22]. In the present paper the calibration curves are realized by employing the AgNPs with different sizes from Nanocomposix company (5, 10, 20, 40, 60, 80 and 100 nm Citrate NanoXactTM Silver). The Nanocomposix NPs are certified by the Company with particle size distribution obtained with TEM analysis. Once obtained the calibration curve of λ_{max} as function of size, an empirical equation to

calculate NPs size of an unknown sample has been retrieved. Then, to measure the concentration of an unknown sample, the extinction coefficient at λ_{max} must to be known in order to apply the Lambert-Beer law ($A=\varepsilon cl$, ε extinction coefficient, c NPs concentration, l path length). Since the extinction coefficient also depends on the NPs size, a calibration curve of $A_{\lambda max}$ as function of known NPs concentration for each NPs size has been performed. Then, extinction coefficient for each NPs size has been calculated. Finally, by plotting the extinction coefficient as function of NPs size, an empirical equation has been also retrieved for calculating extinction coefficient at the size of the NPs under study. The extinction coefficients found with our calibration curves, are comparable with ones measured and calculated in the Supporting Information of ref. [22]. In the table S1, the determined empirical equations of this work are reported as well as an example of size AgNPs distribution performed with TEM images of AgNPs produced with 217 mJ. Even if the determination of NPs size with SPR spectra can be less accurate than the one performed with microscopic techniques, the employment of specific calibration curves performed with own absorbance spectrometer can lead to a good determination of the mean NPs size. In ref. [21, 22] are clearly reported the NPs size determination with both TEM and SPR techniques and the good correlations between the two measurements.

4. Results and discussion

4.1 Cavitation bubble induced on Ag target in water and produced AgNPs

The main processes involved in the PLAL are the laser induced plasma followed by the shock wave (SW) formation, during the first hundreds of nanosecond after the laser pulse, and the induction of the cavitation bubble, whose lifetime is in the order of hundreds of microsecond after the laser pulse, depending on the experimental conditions (the laser fluence, the type of liquid, liquid pressure, etc.[2]). In this work, the temporal evolution of the cavitation bubble induced in water on Ag target at different laser energies and at atmospheric water pressure has been studied. In Fig. S2 and S3 the typical images of laser induced plasma in water followed by the shockwave formation are reported. The experimental conditions are the same of those employed for the cavitation bubble measurements discussed below, but the gate width is 100 ns in order to detect the faster plasma and shockwave evolution. From Fig. S3, the SW velocity was estimated as 1435±14 m/s that is a value similar to the sound speed in water. In Fig. 3 the cavitation bubble dynamics obtained at different laser energies are reported accumulating 5 events. As the accumulation over 5 images of different laser-matter interaction events may reproduce some artifacts due to the chaotic nature of the collapsing phase of the bubble, single shot experiments (see as an example Fig.S4a in the supporting information) have been performed in order to verify the observed features of the bubble dynamics. After confirming the trueness of the observed dynamics, the images obtained with 5 accumulations have been used for the calculation reported below, in order to obtain a more representative average value of the bubble dimension. As already explained above, the bubble formation is due to the fast exchange of energy between the plasma edge and the water surrounding the plasma. During the fast plasma quenching because of the water confinement, water vapor is formed around the plasma. The latter is the starting point of the cavitation bubble. Then the bubble expands until the pressure of the water vapor balances the pressure of the water. The shrinking phase occurs immediately after the maximum of expansion and finishes with the collapse of the bubble. The water vapor pressure at the collapse phase reaches extremely high values, thus leading to a violent collapse of the bubble on the target surface. If enough energy is released during the collapse, a secondary bubble is also generated. In Fig. 3 all the phases described above are shown. Since the lifetime of the bubble strictly depends on the deposited laser energy in the target surface,

it can be noted in Fig. 3 the different times at which the collapse occurs as well as the different dynamics of the secondary bubbles as function of the laser pulse energy.

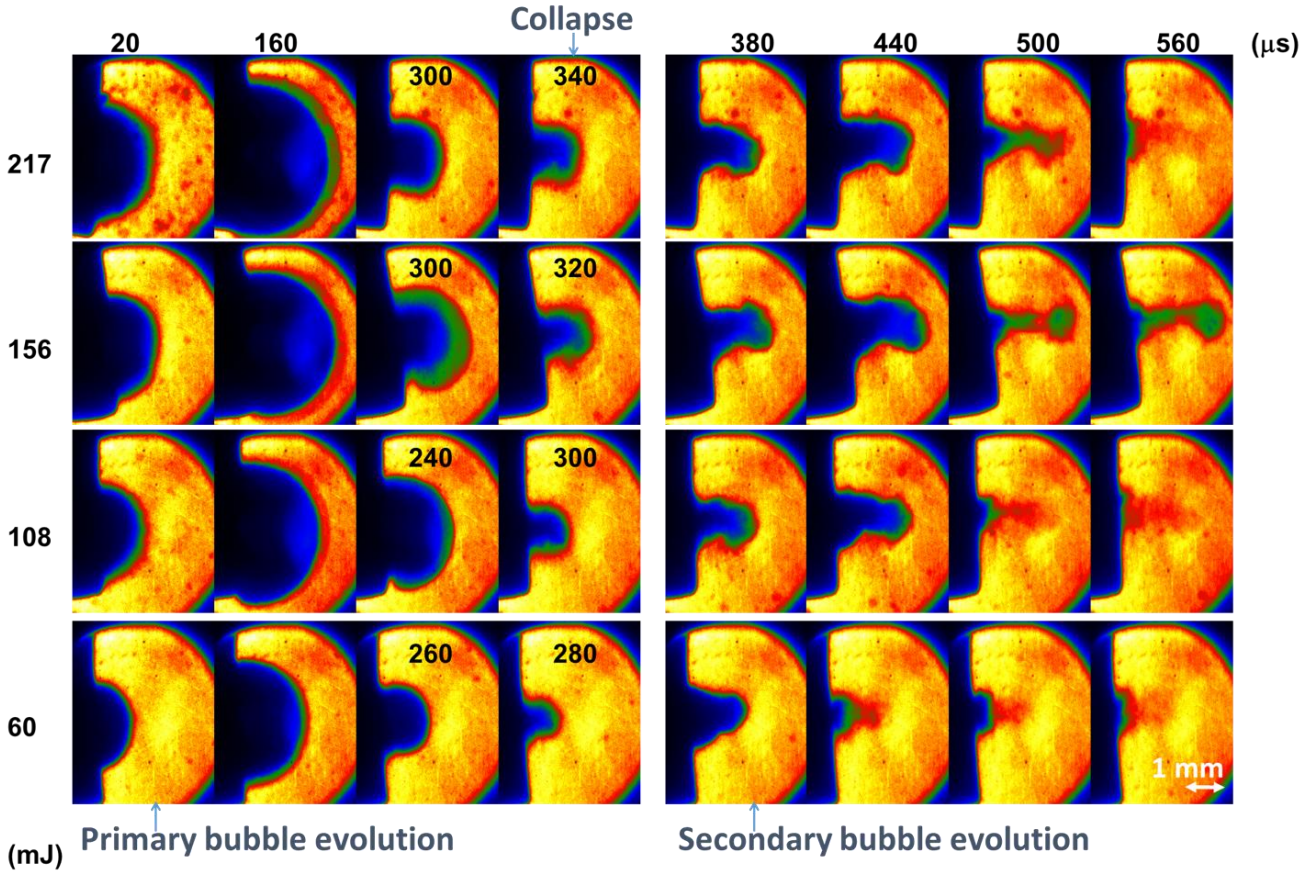

Fig. 3 Temporal resolved shadowgraph images of the laser induced bubble on Ag target immersed in water obtained at different laser energies, 217, 156, 108 and 60 mJ, respectively.

During the evolution of the secondary bubble, shadowgraphs clearly show two distinguishable components: an inner bubble and an outer part with a plume shape. The outer plume assumes an irregular shape, while the inner bubble holds the typical hemispherical shape. In Fig. S4 some other characteristic shadowgraph images of the secondary bubble acquired at different laser energies are reported as well, in order to visualize the double shape in the shadowgraph of the secondary bubble. It is interesting to note that while the radius of the inner bubble perfectly fits the theoretical trend of the cavitation rebounding and collapse phases, the second component after the collapse of the primary bubble, carries on a momentum in the forward direction with respect to the target surface, suggesting an intrinsic propulsion. As it can be seen in Fig. 4, where the front of the bubble outer plume is reported compared to the bubble radius evolution, the speed of the front of the outer plume, after its complete separation from the inner bubble, is similar (with a value around 6.5 m/s) at each employed energies, suggesting that after the initial propulsion the material composing the outer plume is slowed down by the water.

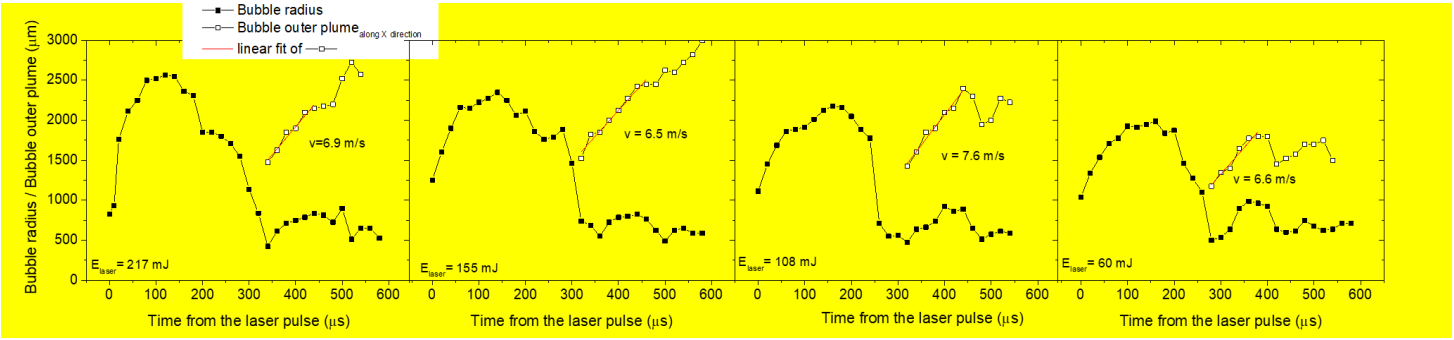

Fig. 4 Laser induced bubble radius produced on Ag target immersed in water at different laser energies (217, 156, 108 and 60 mJ). The front of the bubble outer plume is reported compared to the bubble radius evolution. The speed of the front of the outer plume is measured by the slope of a linear fitting.

Finally, AgNPs have been produced with the same experimental conditions of the cavitation bubbles reported in Fig. 3, and employing a laser ablation time of 15 min and a laser frequency of 10 Hz. In Fig. 5 the corresponding SPR spectra, collected immediately after the PLAL process, are reported. In table 1 the laser energies with the corresponding laser fluences, the average size and the concentration of AgNPs are shown. Since the volume of solution, the ablation time and the laser frequency are known, the number of produced AgNPs for laser shot can be also calculated. Here it may be important to note that the ablated mass is expected to be much higher than the mass of the produced NPs with characteristics like those reported in Table1. Indeed beyond the spherical NPs, bigger particle are ejected during the laser ablation and also some of the material aggregates or coalesces during the various steps of the PLAL process. In any case, for the following discussion we focus our attention just to the spherical NPs that are of main interest for practical applications.

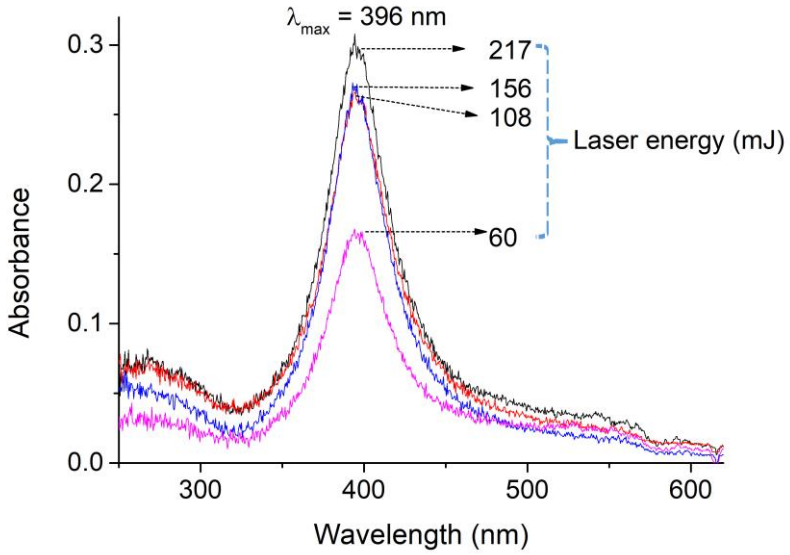

Fig. 5 Surface plasmon resonance spectra of AgNPs colloidal solutions produced with different laser energies.

Table 1 Laser energies with corresponding laser fluences employed for the AgNPs production, averaged size and concentration of AgNPs. The relative errors of NPs size are also reported.

Laser Energy/Fluence (mJ)/(Jcm^{-2})	**Size (nm)**	**AgNPs concentration (n° AgNPs/l)**	**n° AgNPs for laser shot**
217/27.6	7.4 ± 2	8.7 E14	3.76 E10
156/19.9	7.4± 2	7.8 E14	3.38 E10
108/13.7	7.4± 2	7.4 E14	3.27 E10
60/7.6	7.4± 2	2.1 E14	2.08 E10

4.2 Particles releasing from the cavitation bubble to the solution.

Assuming that the NPs are charged, they are subjected to the repulsion due to their electrostatic potential. Being the NPs in a condensed state, they constitute a different physical phase with respect to the gas in the cavitation bubble and so their motion can be considered independently from the gas pressure in the bubble. In this frame, the pressure of the NPs cloud and the vapor in the bubble can be considered independently as they are two distinguished phases. As a first approximation (i.e. neglecting their initial velocity) the pressure of the cloud of NPs in the bubble volume can be considered as the pressure of their total charge at the boundary of the bubble, that is indeed negative as this charge is due to the electron charging. It would be reasonable that after the plasma phase, the NPs hold their electrostatic charge because they are immersed in the gas phase of the cavitation and so they cannot discharge the excess of electrons.

The number of electrons attached to the NPs depends on the NPs size. Larger is the surface, more electrons can be hosted [4]. In a previous work, in the case of AgNPs, has been calculated that, for 10 nm diameter NPs, about 10 electrons are allocated on the particle. In this work, AgNPs with average size of 7 nm are produced at each considered laser energy. An estimation of the number of electrons hosted on AgNPs can be done as in [17] from which it can be assumed that 7 electrons can be hosted on AgNPs with size of 7 nm. By assuming this value, and taking into account that the results shown below are qualitatively not affected by the exact number of electrons per NP in a range of tolerance of 40%, it is possible to estimate the electrostatic pressure of the cloud of NPs at the surface of the cavitation bubble, after the plasma stage, with the following relation based on the electrostatic potential of the negative charged NPs contained within the cavitation bubble at the cavitation bubble boundary (Gauss law):

$$P_{NPs} = \frac{\varepsilon_0}{2}\left(\frac{\sum_n q_n}{4\pi\varepsilon_0}\frac{1}{R_B^2}\right)^2 \qquad \text{eq.3}$$

where ε_0 is the permittivity, the term in the parenthesis is the total electromagnetic field induced by the charged NPs in the bubble volume of radius R_B. In the approximation that all the NPs have the

same size (i.e. the average size determined with SPR) the summation in eq.1 can be replaced with the product of the total number of NPs by the number of electron charges attached to the NPs:

$$\sum_n q_n = N_{NP} \cdot N_{e^-} \qquad \text{eq. 4}$$

It is interesting to compare the electrostatic pressure of the charged NPs with the pressure inside the bubble obtained with the Van der Waals equation as obtained by the measurement of the radius in the experimental images (Fig.3):

$$P(R_B) = \left(P_\infty + \frac{2\sigma}{R_B} \right) \left(\frac{R_\infty^3 - h^3}{R_B{}^3 - h^3} \right)^\gamma \qquad \text{eq.5}$$

In Eqs. 3, P_∞ is the pressure of the liquid, R_B is the bubble radius R_∞, is the radius at which pressure inside the bubble corresponds to the liquid pressure, σ is the surface tension of water, $h=R_\infty/9.174$ is the actual radius estimated taking into account the water molecules covolume, $\gamma = C_p/C_v = 1.31$.

Fig.6 shows the comparison between eqs.1 and 3 for 7 nm NPs charged with 7 electrons in the case of the experiment at laser fluence of 27.6 J/cm^2. The estimation of the initial number of the NPs filling the cavitation bubble during its evolution has been done, in this first calculation, by inserting the experimental number of produced NPs per laser shot as reported in table 1. The latter assumption leads to an under estimation of the real number of the NPs in the bubble, since it does not take into account the smallest fraction of NPs [16] that can be trapped inside the cavitation bubble, but this does not affect qualitatively the following discussion. Fig.6 shows that the electrostatic pressure is higher than the bubble pressure at the maximum of the bubble expansion, while is lower or equal in the initial and final stage of the cavitation bubble evolution. Finally, during the rebound the electrostatic pressure is always higher than the bubble pressure as a consequence of the high repulsion between the NPs compressed in a small volume.

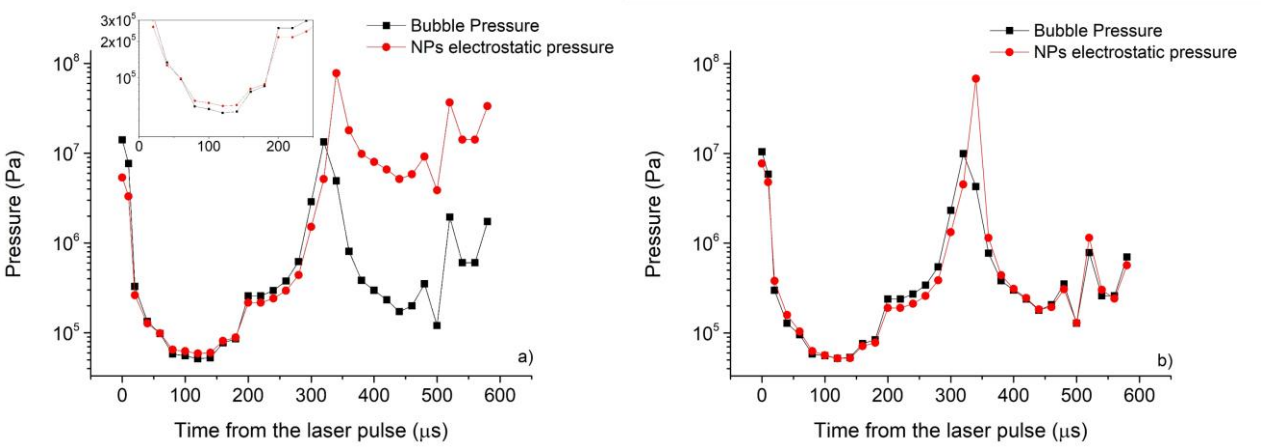

Fig.6. a) Cavitation bubble pressure (eq.5) and electrostatic pressure (eq.3) as function of time from the laser pulse. The experimental bubble radius evolution was measured from shadowgraph images acquired with fluence F=27.6 J/cm^2. An initial number of NPs 3.76 10^{10} with 7 electrons on NPs surface have been considered in the electrostatic pressure calculation. In b) the calculation of electrostatic pressure has been performed by taking into account the variation of the number of NPs inside the bubble as a consequence of their releasing in solution during the bubble evolution.

Considering that the pressure of the cavitation bubble is equal to that one of the liquid at the bubble interface, if the electrostatic pressure is higher than that one of the cavitation bubble, NPs escape from the bubble, for decreasing the repulsion between each other and, in turn, the electrostatic pressure. The fraction of NPs that leaves the bubble is the one that allows the equilibrium between the electrostatic pressure and the pressure at the border of the cavitation. In other words, when the NPs clouds pressure is greater than the pressure of the liquid at the cavitation bubble border, NPs cannot be confined anymore and are released in the solution. On the contrary, if the pressure at the bubble border is larger than the electrostatic pressure, the NPs remain confined inside the cavitation. In this view it is possible to estimate the amount of NPs delivered in the solution by assuming that for each time the NPs cloud releases charged NPs in the solution in order to reach the same pressure of the bubble at the subsequent instant. We simultaneously calculate at each time the number of NPs released in solution putting in equilibrium P(R_B) and P(NPs) and, at subsequent instant, the electrostatic pressure by inserting in the equation the remaining number of NPs inside the bubble. The pressure of the NPs cloud tends to be closer to that one of the cavitation bubble as reported in Fig 6b. Moreover, to simulate a more realistic situation, by an iterative calculation (see supporting information), we have set the initial number of NPs contained in the bubble, in order to obtain the number of the total ejected NPs equals to the number of NPs per shot experimentally measured immediately after the ejection in solution. The value inserted at the beginning of the bubble expansion corresponds to an excess of about 20% with respect to the number of NPs released in the solution as will be discussed below. In Fig. 7 the calculated number of AgNPs released in solution and inside the bubble, respectively, are shown and they are compared with the experimental radius of the cavitation bubble as function of time. By the inspection of Fig. 7, it is visible that, by decreasing the laser fluence the maximum bubble radius decreases as well as the time at which the collapse occurs, as it is also visible in Fig. 3.

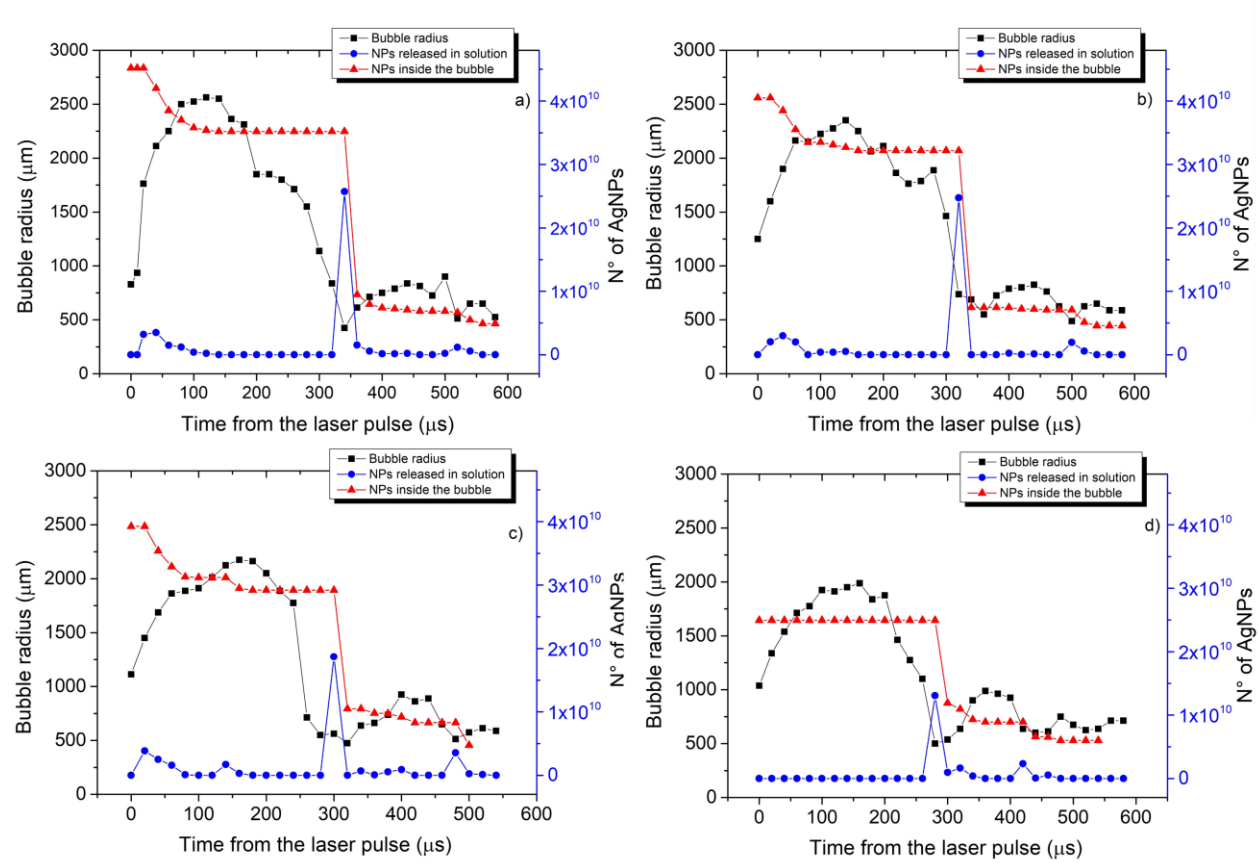

Fig.7. Number of NPs inside the bubble and number of ejected NP, reported with the bubble radius as function of time from the laser pulse at different laser energies a) 217 mJ, b)156 mJ, c) 108 mJ and d) 60 mJ, respectively.

Nevertheless, the behavior of the AgNPs released in solution is similar, even if the number of the ejected particles is different during the bubble evolution for each considered laser fluence. In particular, Fig.7 shows a characteristic trend, where the two main ejection streams of NPs are located at the initial stage of the bubble expansion and after the collapse. In Fig. 8a the calculated number of AgNPs released in solution at two employed laser fluences is shown as percentage of the initial number of AgNPs filling the bubble. In Fig. 8b the corresponding bubble radii evolution with the outer plume fronts are also reported. In Fig. S6, the percentages of ejected AgNPs at all laser fluences employed in this work can be found. Fig. 8a shows that NPs start to escape from the bubble as soon as the electrostatic pressure become greater than the bubble pressure. The time of the first AgNPs ejection depends on the laser fluence and, in turn, on the bubble radius and it is between 50 and 150 μs. In the case of the lower laser energy no NPs delivering is revealed before the collapse stage, while in the case of the highest laser energy, a releasing of NPs between 5 and 10% occurs. After the first NPs ejection, when the electrostatic pressure equals the one of the bubble, NPs releasing stops as the remaining NPs can be confined inside the bubble for almost the all bubble evolution. Finally, immediately after the collapse stage, the pressure in the rebound bubble is notably lesser than the electrostatic pressure and the NPs are released again in the solution in a greater amount. At the end of the process about the 80% of the NPs have been delivered in the liquid, while the remaining 20% are trapped inside the bubble.

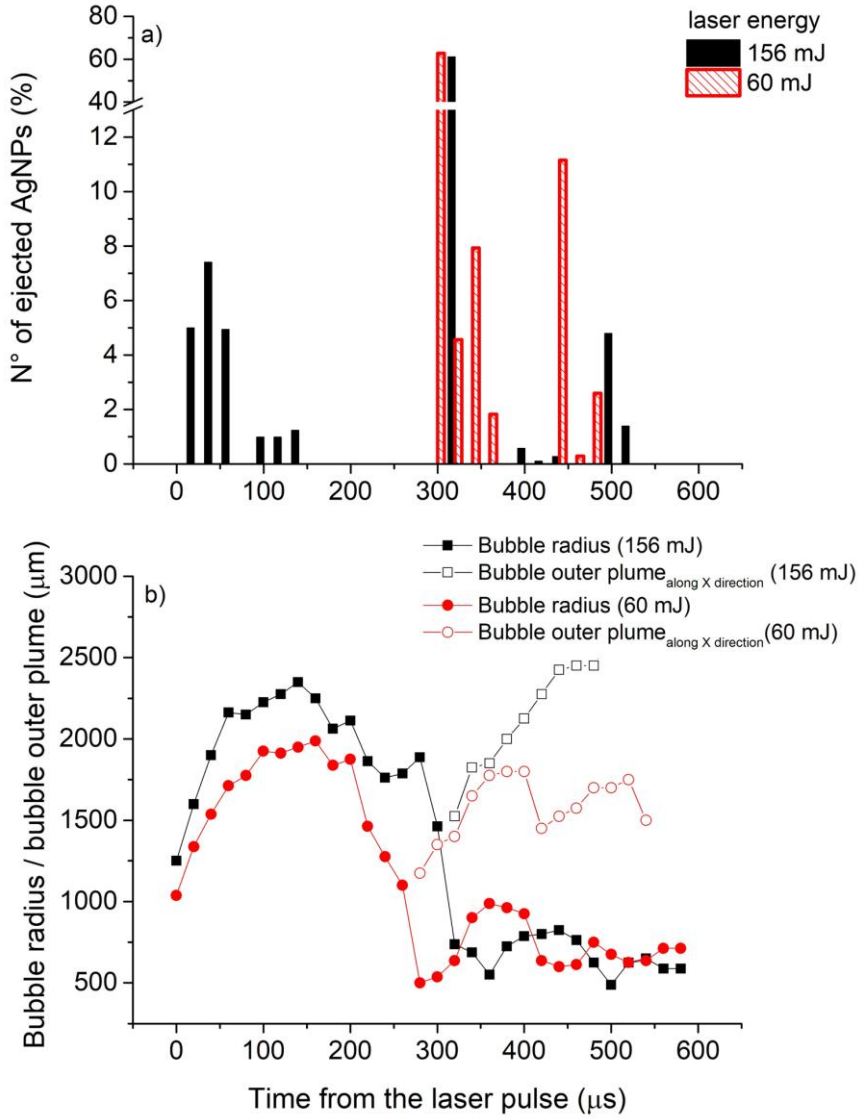

Fig. 8 a) Percentages of ejected AgNPs as a function of time after laser pulse calculated at two laser energies (156 and 60 mJ) and b) the corresponding bubble radii and bubble outer plumes evolution.

It is interesting to note that, in agreement with many observations in literature [23], NPs are mostly confined inside the bubble until the bubble rebound. This was observed in a previous experiment [24, 3] where a second laser pulse induced a secondary plasma on the cloud of NPs clearly locating the position of the NPs inside the cavitation bubble. The experimental details of the mentioned experiments are described in ref [24] and are summarized in the Fig.9 caption. In Fig.9 a and b, it is shown the images obtained by a fast camera using a second laser pulse suitably delayed with respect to the ablation one (Interpulse Delay, I. D.). The first laser pulse induces a bubble and the second pulse is employed in order to probe the material inside the bubble at different times of the bubble evolution reported in Fig.9c. By the inspection of Figs.9 it is possible to see that, after 80 μs, within the primary plasma due to the laser target interaction, a secondary plasma on the NPs cloud is induced by the second laser pulse. It is also possible to see a third plasma outside the bubble induced on the ejected NPs from the bubble. Since the secondary plasma is completely inside the cavitation, the most part of the NPs are still confined inside the bubble. Finally, after 200 μs, that

corresponds to the bubble rebound stage, the cloud of NPs is completely outside the bubble as it is shown by the irregular plasma induced on the material in the liquid phase. These observations agree with the model of the NPs releasing discussed in this paper. For instance, in Fig. 9c, the eq. 3 and 5 have been applied to the bubble radius measured during that experiment [24] and by taking into account the AgNPs produced during the single pulse laser ablation. In agreement with Ref. [24], the AgNPs produced in these last conditions were found of 6 nm size and with an estimated number of NPs of 1.3 10^{10} for laser shot. For performing the calculation described above, 6 nm NPs were considered charged with 5 electrons [17]. Also in this case an iterative method has been applied in order to obtain the same number of the calculated ejected NPs as that one found experimentally in the solution. The results of the proposed model are in agreement with the experimental observation shown in Fig. 9a-c denoting the robustness of the proposed approach and of the general phenomena discussed in the present paper.

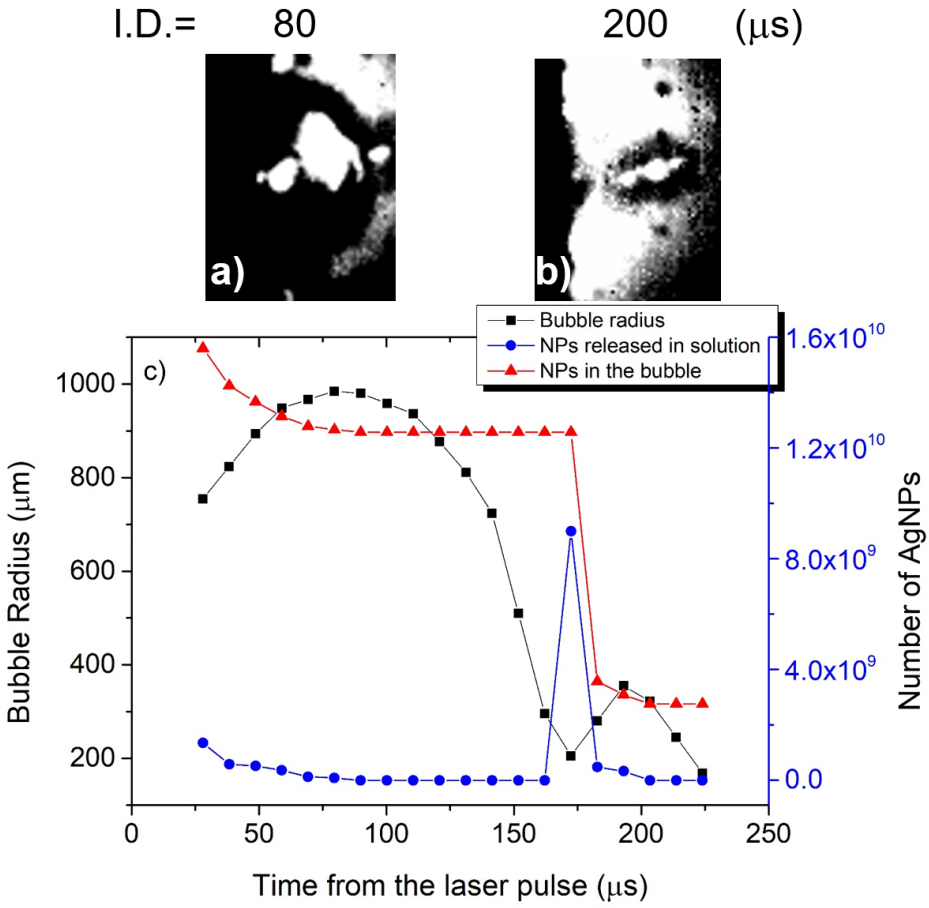

Fig. 9 Some frames of shadowgraph images collected with a fast camera during double pulse probing at different time evolution of the cavitation bubble with respect to the laser ablation pulse (Interpulse delay between the two laser pulses: I. D.): a) I. D. = 80 μs (before the maximum expansion); b) I. D. = 200 μs (during bubble rebounding). In c) the bubble radius as measured from shadowgraph images during a single-pulse LAL experiment, the calculated number of AgNPs inside the bubble and the calculated number of ejected AgNPs as function of the time from the first laser pulse are reported (λ_{laser} = 532 nm, irradiance = 17.5 GW cm^{-2}, gate width of a) and b) = 81 μs, gate width of c) = 28 μs. Experimental set-up is described in ref. [24]).

Conclusions.

In this paper the role of plasma charging on NPs produced by PLAL has been discussed. Considering that whatever is the main process of NPs growth, NPs formed in the plasma are negatively charged, the charge effect has been investigated in order to model the releasing of NPs in solution. In this frame the electrostatic pressure of the NPs cloud has been compared with the pressure of the cavitation bubble. In order to balance the NPs electrostatic pressure and the pressure inside the bubble, the excess of charged NPs has been considered ejected from the cavitation bubble. This result allows estimating the amount of NPs released in solution as well as the dynamics of the ejection. This scenario, although very simple, as we are neglecting the NPs transport phenomena inside the bubble and the liquid, underlines as NPs can be ejected from the bubble environment as faster as the difference between the electrostatic and the bubble pressure is greater. Finally, as already discussed in previous works, the NPs are therefore released in solution with a negative charge due to the absorbed electrons. This excess of charge can be an important contribution to the impressive stability of the colloidal solutions produced by ns-PLAL without the support of chemical stabilizers.

References:

1. Dell'Aglio M., Alrifai M, De Giacomo A, 2018, Nanoparticle Enhanced Laser Induced Breakdown Spectroscopy (NELIBS), a first review, Spectrochimica Acta Part B, 148 105–112
2. Kanitz A., Kalus M-R, Gurevich E. L., Ostendorf A., Barcikowski S, Amans D, 2019, Review on experimental and theoretical investigations of the early stage, femtoseconds to microseconds processes during laser ablation in liquid-phase for the synthesis of colloidal nanoparticles, Plasma Sources Sci. Technol., 28, 103001
3. Dell'Aglio M., Gaudiuso R., De Pascale O., De Giacomo A., 2015, Mechanisms and processes of pulsed laser ablation in liquids during nanoparticle production, Applied Surface Science, 348, 4-9
4. Taccogna F., Dell'Aglio M., Rutigliano M., Valenza G., De Giacomo A., 2017, On the growth mechanism of nanoparticles in plasma during pulsed laser ablation in liquids, Plasma Sources Science and Technology, 26 (4), 045002.
5. Dell'Aglio M., Motto-Ros V., Pelascini F., Gornushkin I.B., De Giacomo, A., 2019, Investigation on the material in the plasma phase by high temporally and spectrally resolved emission imaging during pulsed laser ablation in liquid (PLAL) for NPs production and consequent considerations on NPs formation, Plasma Sources Science and Technology, 28 (8), 085017.
6. Taccogna F., Nucleation and growth of nanoparticles in a plasma by laser ablation in liquid, 2015, Journal of Plasma Physics, 81 (5), 495810509
7. Ibrahimkutty S, Wagener P, Menzel A, Plech a, Barcikowski S, 2012, Nanoparticle formation in a cavitation bubble after pulsed laser ablation in liquid studied with high time resolution small angle x-ray scattering, Appl. Phys. Lett. 101, 103104
8. Reich S, Schönfeld P, Wagener P, Letzel A, Ibrahimkutty S, Gökce B, Barcikowski S, Menzel S, dos Santos Rolo T, Plech A, 2017, Pulsed laser ablation in liquids: Impact of the bubble dynamics on particle formation, Journal of Colloid and Interface Science 489, 106–113.
9. Shih C. Y, Streubel R, Heberle j, Letzel A, Shugaev M V, Wu C, Schmidt M, Gökce B, Barcikowski S, Zhigilei L V, 2018, Two mechanisms of nanoparticle generation in picosecond laser ablation in liquids: the origin of the bimodal size distribution, Nanoscale, 10, 6900

10. Girault M et al 2016 Influence of the reactive atmosphere on the formation of nanoparticles in the plasma plume induced by nanosecond pulsed laser irradiation of metallic targets at atmospheric pressure and high repetition rate Appl. Surf. Sci. 374 132–7
11. Kim M, Osone S, Kim T, Higashi H, Seto T, 2017, Synthesis of Nanoparticles by Laser Ablation: A Review, KONA Powder and Particle Journal, 34, 80-90
12. Lavisse L et al 2012 In-situ small-angle x-ray scattering study of nanoparticles in the plasma plume induced by pulsed laser irradiation of metallic targets Appl. Phys. Lett. 100 164103
13. Povarnitsyn, M.E., Itina, T.E., Levashov, P.R., Khishchenko, K.V., 2013, Mechanisms of nanoparticle formation by ultra-short laser ablation of metals in liquid environment, Physical Chemistry Chemical Physics, 15 (9), pp. 3108-3114.
14. Goree J 1994 Charging of particles in a plasma Plasma Sources Sci. Technol. 3 400–6
15. Ibrahimkutty S, Wagener P, dos Santos Rolo T, Karpov D, Menzel A, Baumbach T, Barcikowski S, Plech, 2015, A hierarchical view on material formation during pulsed-laser synthesis of nanoparticles in liquid, Scientific RepoRts, 5:16313
16. Dell'Aglio M, Santagata A, Valenza G, De Stradis A and De Giacomo A 2017 Study of the effect of water pressure on plasma and cavitation bubble induced by pulsed laser ablation in liquid of silver and missed variations of observable nanoparticle features ChemPhysChem 18 1165–74
17. Palazzo G, Valenza G, Dell'Aglio M, De Giacomo A, 2017, On the stability of gold nanoparticles synthesized by laser ablation in Liquids, Journal of Colloid and Interface Science 489, 47–56
18. Seto T, Kawakami Y, Suzuki N, Hirasawa M, Aya N, 2001, Laser Synthesis of Uniform Silicon Single Nanodots, NANO LETTERS, 1, 6 315-318
19. Li N, Guo J, Lin Zhu, Lu Y, Tian Y, Zheng, 2019, Effects of Ambient Temperature on Laser-Induced Plasma in Bulk Water, Applied Spectroscopy, 73(11) 1277–1283
20. Dell'Aglio M., Mangini V., Valenza G., De Pascale O., De Stradis A., Natile G., Arnesano F., De Giacomo A., 2016, Silver and gold nanoparticles produced by pulsedlaser ablation in liquid to investigate their interaction with ubiquitin, Appl. Surf. Sci. 374, 297–304.
21. Haiss W., Thanh N.T.K., Aveyard J., Fernig D.G., 2007, Determination of size and concentration of gold nanoparticles from UV-vis spectra, Anal. Chem. 79, 4215–4221.
22. D. Paramelle, A. Sadovoy, S. Gorelik, P. Free, J. Hobleya, D. G. Fernig, A rapid method to estimate the concentration of citrate capped silver nanoparticles from UV-visible light spectra, Analyst, 2014, 139, 4855
23. Kudryashov S. I., Samokhvalov A. A., Nastulyavichus A. A. , Saraeva I. N. , Mikhailovskii V. Y.,. Ionin A. A., Veiko V. P., 2019, Nanosecond-Laser Generation of Nanoparticles in Liquids: From Ablation through Bubble Dynamics to Nanoparticle Yield, Materials, 12, 562
24. Dell'Aglio M, Gaudiuso R, ElRashedy R, De Pascale O, Palazzo G, De Giacomo A, 2013, Collinear double pulse laser ablation in water for the production of silver nanoparticles, Phys.Chem. Chem. Phys., 15, 20868